



24 always be easily reached because of a structure of the soil that is difficult to break down at the  
25 strains applied by standard laboratory tests. Some authors have therefore defined different  
26 critical state lines in the volumetric plane for natural and reconstituted samples of the same soil  
27 (e.g. Cotecchia & Chandler, 2000; Hosseini-Kamal et al., 2014) because the volumetric states  
28 at the ends of their tests are reasonably stable and can be regarded as pseudo critical states. For  
29 some soils this is simply a pragmatic choice and it could be envisaged that much larger strains  
30 or other types of loading might give convergence, but in others very robust forms of natural  
31 fabric can only be broken down by very severe mechanical remoulding (e.g. Fearon & Coop,  
32 2000).

33 In reconstituted soils the fabric created by the preparation method often has an effect on  
34 subsequent behaviour (e.g. Santucci et al., 1998; Madhusudhan & Baudet, 2014). These effects  
35 may be related to, but should not be confused with, the so-called “transitional” behaviour in  
36 which the initial specific volume of a sample has a persisting effect on the subsequent  
37 behaviour, often regardless of preparation method. In these cases standard laboratory tests such  
38 as oedometers or triaxials may give locations of the normal compression and critical state lines  
39 that appear to depend on the initial density. Samples that have different specific volumes at  
40 similar stress states must have different fabrics, but Shipton & Coop (2015) found that for the  
41 simple sand / kaolin mixed soil, the sample preparation technique per se had no significant  
42 influence beyond the initial sample densities that they enabled to be created.

43 While the soils that have been used in the work described in this paper are simple laboratory  
44 created mixtures of fairly standard soil particles, this transitional behaviour has also been  
45 reported in reconstituted samples of natural soils, for example saprolites, alluvial and lagoon  
46 sediments, glacial till and natural sands (Ferreira & Bica, 2006; Nocilla et al., 2006; Ponzoni  
47 et al., 2014; Altuhafi et al., 2010; Ventouras & Coop, 2009) as well as a number of “man-  
48 made” materials such as mine tailings and rock fill (Coop, 2015; Xiao et al., 2016). In some of

49 these materials standard tests seem to give normal compression or critical state lines that are,  
50 to all intents and purposes, parallel, while in others a slow convergence with increased stress  
51 level is clear, but often without the possibility that a unique normal compression or critical state  
52 line is defined before the zero void asymptote is approached. While all “transitional soils” must  
53 have an influence of initial density on the compression behaviour, some seem to give better  
54 convergence for critical states, indicating that volumetric and shear strains both affect the  
55 convergence but perhaps differently (Ponzoni et al., 2014).

56 The subject of transitional soils provokes controversy as it challenges some of our common  
57 assumptions and the idea that fabrics in reconstituted soils can have such persistent effects  
58 seems to be less readily accepted than for natural soils. The fact that it has proven impossible  
59 to predict which soils might be transitional and which not simply from grading has added to  
60 the apparent complexity, even if Ponzoni et al. (2017) have recently shown how mineralogy  
61 and grading may interact to cause it. The purpose of this paper is to navigate a way out of the  
62 complexity of these complex and often apparently contradictory data, hopefully offering a  
63 means to break through entrenched positions on how we should interpret the behaviour. Data  
64 from examples of “transitional soils” are first used to illustrate the problems of identifying  
65 unique behaviour and then a means of quantifying the rates of convergence to unique  
66 volume/stress states is given that allows comparison between data from different types of  
67 loading, highlighting when and how convergence might be brought about.

## 68 Materials and Testing

69 The materials used were not chosen to represent any particular natural soil and exactly what  
70 soils were tested is not of especial relevance because they were chosen mostly as examples that  
71 would clearly demonstrate the methods proposed in this paper. Even so, the gap graded soil  
72 was initially chosen by Martins et al. (2001) to have a similar grading to their natural saprolite.

73 This soil, of 75% quartz sand and 25% kaolin, was extensively tested by Shipton & Coop (2012,  
74 2015) who used Thames valley sand for the quartz fraction (Takahashi & Jardine, 2007),  
75 highlighting normal compression lines and critical state lines in the  $e: \ln p'$  ( $e$  void ratio,  $p'$  mean  
76 normal effective stress) plane that they interpreted as parallel and dependent on initial density.  
77 The raw data and testing details for this soil are not repeated here, as only a few new tests were  
78 needed to fill gaps in the existing data and details of procedure and data are given in Shipton  
79 & Coop (2012, 2015). This soil is referred to as sand with plastic fines (SPF).

80 The other two soils were based on the fractally graded sands that Altuhafi & Coop (2011)  
81 showed had transitional, or non-convergent, compression behaviour in oedometer tests, even  
82 at stresses over 100MPa. The gradings of the quartz and crushed limestone sands were not quite  
83 the same as those Altuhafi & Coop used, because the large amounts of soil needed here meant  
84 that the finer end of the grading could not be controlled to be fractal, but was simply created  
85 by adding commercial quartz or calcium carbonate silts. The quartz sand was Leighton Buzzard  
86 sand (LBS) and the crushed limestone (LMS) was supplied from China. The coarser part of the  
87 grading was controlled to be fractal using the mass method between 63 and 600 $\mu\text{m}$  with a  
88 fractal dimension of 2.57, as for Altuhafi & Coop. The gradings of all three soils are shown in  
89 Fig.1. Soils that are nominally fractal, like this, may seem to be purely artificial, but Coop et  
90 al. (2004) found that intense shearing would give a terminal grading of this type and they occur  
91 naturally in tills sheared under glaciers (Altuhafi et al., 2010).

92 The tests carried out were relatively straightforward, a key motivation behind the work being  
93 to see what compatibility there is between the degrees of convergence in different types of  
94 simple test. The oedometer tests, summarised in Table 1, were generally carried out in 50mm  
95 diameter fixed rings, but to reach the highest stresses smaller diameters of 30 or 20mm were  
96 used, but these had a floating ring design to minimise wall friction.

97 Three different triaxial apparatus were used, each of a stress path type, one with GDS pressure/  
98 volume controllers with a sample size of 50mm diameter and 100mm height and two using  
99 Imperial College pneumatic control systems with sizes of 50mm diameter and 100mm height  
100 and 38mm diameter and 76mm height. The volumetric strains were measured either with the  
101 GDS controller or Imperial College volume gauges and the axial strains both by local LVDTs  
102 attached to the samples and an external LVDT mounted outside the cell chamber. Because of  
103 the large strains needed to examine whether unique critical states could be reached, only the  
104 external LVDT data are presented here, but the internal strain data showed good agreement up  
105 to the point where they went out of their measuring range. Also because of the large strains, a  
106 suction cap (Atkinson & Evans, 1985) was used to hold the sample firmly to the axial loading  
107 system, ensuring that it remained upright and concentric. Good saturation, with B values over  
108 96%, was achieved by carbon dioxide circulation prior to water saturation, followed by the  
109 application of back pressures over 200kPa. For the LBS and LMS soils shearing was started at  
110 0.05%/h at axial strains below 0.1%, to achieve good definition of the small strain stiffnesses,  
111 although these data are not discussed here. The rates were then gradually increased to a  
112 maximum of 0.4%/hour at large strains. Similar strain rates were used in drained and undrained  
113 tests, but the LMS and LBS soils were free draining and the slower rates at the start of the tests  
114 were only to ensure that the small strain data could be collected. The strain rates were only  
115 increased gradually to avoid large accelerations, while reaching a speed that was fast enough  
116 to finish each test in reasonable time, each shearing stage test typically lasting 3-4 days overall.

117 Even if the bulk of the triaxial tests in Tables 2 and 3 were of a fairly standard type, several  
118 tests using lubricated end platens were carried out in the LBS to verify the conclusion of  
119 Shipton and Coop (2015) that they did not make a significant difference. This is not to say that  
120 lubricated end platens are not an important means of improving test quality, just that within the  
121 large void ratio differences seen by Shipton & Coop, their effect was secondary. The high

122 compressibility of the soils during both isotropic compression and subsequent shearing meant  
123 that in some cases the strains that could be reached in shearing were limited by the available  
124 stroke of the apparatus, and these are highlighted in the tables.

125 The LBS and LMS samples were all made by dry compaction, using under-compaction, since  
126 water pluviation led to segregation and layering while wet compaction gave rise to high  
127 suctions in the LMS. Some additional tests to fill gaps in the data for SPF utilised moist  
128 compaction or making samples by compression of a slurry, but as Shipton & Coop (2015)  
129 showed, the preparation method does not affect whether or how quickly the volume states  
130 converge in this soil. All of these samples were visually homogeneous. The compaction used  
131 for each sample varied because a wide range of different initial void ratios was required, and it  
132 was not required for all of them to have the same initial value. The initial void ratio of each  
133 sample is given in Tables 1-3.

134 A particular problem with transitional soils has been the identification of the fabric that gives  
135 rise to the slow convergence, particularly since the wide range of particle sizes means that it is  
136 difficult to know at what scale to examine the fabric with techniques such as SEM (e.g. Nocilla  
137 et al., 2006). However, Mercury Intrusion Porosimetry allows a wide range of scales to be  
138 investigated simultaneously, and Todisco et al. (2018) used this method to determine that for  
139 each soil discussed here there is a micro-fabric that is difficult to break down in conventional  
140 laboratory tests. Isotropy of the shear moduli measured with bender elements also indicated  
141 that the fabrics are isotropic and so they must be heterogeneous at the micro-scale.

142 Quantifying convergence is critically dependent on the accuracy of the void ratio  
143 measurements. The philosophy adopted here, as in previous similar work on transitional soils,  
144 was that it was not adequate just to evaluate that accuracy from the estimated accuracy of  
145 individual measurements made, such as weights or dimensions, which typically gives an

146 optimistic assessment. Instead, a positive verification is made by means of multiple  
147 measurements of void ratio on the same sample, utilising dimensions and weights both at the  
148 start and end of each test that were as independent as possible, along with the measured  
149 volumetric strains during testing, as described by Rocchi & Coop (2014). At least three  
150 measurements were therefore made of the initial void ratio of each sample and the accuracy  
151 estimated from the difference between the highest and lowest value, discarding tests where the  
152 accuracy was worse than  $\pm 0.03$ . The specific gravities measured were respectively 2.61, 2.72  
153 and 2.64 for the LBS, LMS and SPF.

154

#### 155 Compression and Shearing Data

156 Isotropic and oedometric compression data are given in Fig.2 for the LBS and LMS soils. The  
157 data for the SPF soil were presented in detail by Shipton & Coop (2015) and are not repeated  
158 here. In both cases the compression curves steepen slowly and in neither case are there well  
159 defined yield points and unique normal compression line as might be expected in, for example,  
160 a uniformly graded sand at higher stresses (e.g. Coop & Lee, 1993). In isotropic loading there  
161 is little convergence of the compression paths, but in one-dimensional loading there is more,  
162 partly because of the higher stresses reached, but also because yield in oedometric compression  
163 would be expected at a lower stresses than for isotropic. However, there is little space  
164 remaining at very high stresses in the  $e:\log\sigma'_v$  plane between the ends of the oedometer tests  
165 and the zero asymptote for any normal compression line to exist. The isotropic compression  
166 tests with and without lubricated end platens do not differ significantly within the context of  
167 this lack of convergence.

168

169 Example shearing stress-strain data for the LMS soil are given in Fig.3; space precludes giving  
170 all the data for the LMS soil and so tests with a range of effective cell pressures, different initial  
171 void ratios and both drained and undrained are given. The raw data for the LBS are also not  
172 shown, but these were very similar in nature. For brevity only the volumetric strains  $\epsilon_v$  for the  
173 drained tests are given, since the undrained stress paths are given in Fig.4. The shear strain,  $\epsilon_s$ ,  
174 has been defined as:

$$175 \quad \epsilon_s = \epsilon_a - \epsilon_v/3 \quad (1)$$

176 where  $\epsilon_a$  is the axial strain. In each case an indication of the range of initial void ratio,  $e_i$ , values  
177 for the various tests is given so that effects of sample density may be identified more easily.  
178 For clarity the stress-strain data are separated into separate plots for looser and denser samples.  
179 There is of course some scatter in the data and some tests were less complete than others due  
180 to apparatus limitations. However, most of the tests do reach large shear strains and in each  
181 case the volumetric strains become reasonably constant.

182 While the key point of discussion of this paper is the lack of convergence to unique volumetric  
183 states, with some scatter the loose and dense samples do reach unique stress ratios. But perhaps  
184 the most noticeable feature of the data is that there is a surprisingly small range of behaviour  
185 for the different densities, most of the samples being mildly compressive with relative small  
186 volume changes and no peak strengths. None of the samples showed any clear visible strain  
187 localisation, as might be expected from their compressive, strain-hardening mode of behaviour.  
188 The lack of diversity of behaviour will be shown to be related to the slow convergence towards  
189 a unique critical state line. But this should not be thought typical of all well-graded soils and  
190 using similar simple apparatus and techniques the usual clear unique critical state line can  
191 generally be observed in the  $e:\ln p'$  plane (e.g. Vilhar et al., 2013), with behaviour ranging from



192 strain-hardening and compressive to dilative and strain-softening, depending on the initial state  
193 parameter.

194 The paths followed by the tests are given in the  $q':p'$  and  $e:\ln p'$  planes in Figs.4 and 5. A unique  
195 critical state line is clearly defined in stress space, irrespective of initial density, the final value  
196 of  $q'/p' = M$  being reached at only 15-20% axial strain. The stress paths for the higher pressure  
197 tests are omitted on Fig.4 for brevity, but they defined the same  $M$  values. In contrast, the paths  
198 followed in the volumetric plane do not converge to a unique critical state line within the range  
199 of strains that could be applied, even allowing for a few highlighted tests that are less complete.  
200 The volumetric strains were reasonably constant at the end of almost all of the tests, so it is  
201 difficult to see what strains might be needed to achieve full convergence. The lubricated end  
202 platens used for some of the LBS tests do not make a significant difference to this pattern of  
203 behaviour. The degree of convergence does seem better at larger stresses but it is clear that  
204 fully convergent paths could not be expected from triaxial tests until stress levels in the 100s  
205 of MPa, at which point there would again be little available room in the  $e:\ln p'$  plane to fit a  
206 useful critical state line before the zero asymptote is approached.

207 Observing similar behaviour for the SPF soil, Shipton & Coop (2015) made the pragmatic  
208 choice to define pseudo critical states at the end of test states, so that a different critical state  
209 line could be identified in the  $e:\ln p'$  plane for groups of samples with similar initial void ratios.  
210 The approach adopted here is to avoid any such controversial choices, and simply to quantify  
211 the rate at which convergence is occurring so that it can be estimated when unique volumes  
212 might be achieved.

### 213 Quantifying Convergence

214 To cope with data that were similarly difficult to interpret, Ponzoni et al. (2014) proposed  
215 quantifying convergence using two methods. The first was simply to take the starting and

216 ending void ratios of oedometer tests and quantify to what extent initial differences of void  
217 ratio were preserved at the highest stress reached. This was done by plotting the initial void  
218 ratios against those at the highest stress level reached, and calculating a gradient of that graph.  
219 Convergence to a unique normal compression line would mean that the final void ratios would  
220 be independent of the initial values so this gradient would be zero, while compression paths  
221 that had no convergence at all would give a gradient of 1, since the final void ratios would be  
222 directly dependent on the initial values.

223 The second method was to take the apparent critical states from the ends of triaxial tests where  
224 reasonably constant volumes had been reached and assume that tests on samples that had had  
225 different initial void ratios had reached different critical state lines at the end of shearing in  
226 the  $e:\ln p'$  plane. The gradients of the critical state lines,  $\lambda$ , were all assumed to be the same, but  
227 each with a different intercept at 1kPa,  $\Gamma$ . The method then quantified how the  $\Gamma$  values changed  
228 with the initial void ratios of the samples.

229 There were several difficulties of these methods. Firstly it had been assumed, if only  
230 pragmatically, that  $e:\ln p'$  critical state lines did exist, even if it was recognised that additional  
231 straining might cause more convergence. Secondly, these were assumed to be linear, which  
232 they might not be. Both methods were tied to quantifying convergence at specific states of the  
233 tests, i.e. the maximum stress reached in the oedometer or the maximum strain in the triaxial,  
234 rather than quantifying the progression of convergence as the tests proceeded. There was also  
235 no means of direct comparison between the two methods. The method proposed here  
236 overcomes these difficulties.

### 237 *Quantifying Convergence in Compression*

238 The rates of convergence are first discussed for the oedometric compression data. The method  
239 is identical for isotropic compression and the graphs for these stages are omitted for brevity as

240 there is less convergence for them because of the lower stresses they reached. For each soil, in  
241 Fig.6 the current void ratio at any load level of a test is plotted against the initial void ratio,  $e_i$ ,  
242 which is generally taken to be as close to a  $p'$  of 20kPa as possible for both the oedometer and  
243 triaxial tests for consistency. In some cases, notably the high pressure triaxial tests the initial  
244 stresses were a little higher than 20kPa, but the compression curves show that this makes only  
245 a small difference in the void ratio. The values of  $p'$  for the oedometer data in Fig.6 assumed a  
246 coefficient of earth pressure at rest,  $k_0=1-\sin\phi'$ . For each soil, examples are given of data for  
247 four different load levels; many more were considered but they are omitted from Fig.6 for  
248 clarity. For each stress level a best fit “convergence line” is determined by linear regression,  
249 the gradient of which,  $m$ , is calculated, the equations being given on the plots. This is similar  
250 to the method of Nocilla et al. (2006) and Ponzoni et al. (2014), the only difference being that  
251 the value of  $m$  is calculated at the various stress levels during the tests rather than solely at the  
252 end.

253 The values of the gradient  $m$  in Fig.6 decrease fairly consistently with increasing stress level  
254 indicating a slow but consistent convergence;  $m=0$  would indicate full convergence to a unique  
255 normal compression line, but in no case is this reached. Within the slight data scatter there is  
256 no noticeable effect of the method of sample preparation for the SPF, as was concluded by  
257 Shipton & Coop (2015). In each case the data are well fitted by straight lines, but it is possible  
258 that this might not be the case for all soils and all possible values of  $e_i$ .

259 For the oedometer tests linear regression fits the data quite well on Fig.6, the data scatter is  
260 acceptable, and the decrease of gradient with increasing stress level is consistent. The same  
261 was true for the isotropic compression data. However, for the triaxial shearing data it is far  
262 more difficult to achieve such consistent data, as will be discussed below, and the gradients of  
263 the convergence lines were not so consistent, so that attempts were made to constrain the  
264 values. One possible means of constraint, shown for two example stress levels for each soil, is

265 to force all of the chosen lines to pass through the origin. The equations for these are also shown  
266 on the figures. This constraint gives lines for the oedometer tests that fit reasonably well for  
267 the LMS and SPF soils, but poorly for the LBS. The consequence of such an assumption is that  
268 complete convergence of the compression paths for different initial void ratios to reach  $m=0$   
269 would only occur as the zero voids asymptote is approached, which may be correct for some  
270 soils but may not be for others.

271 The values of  $m$  from the isotropic and one-dimensional compression tests are plotted against  
272  $\log p'$  in Fig.7. Gradients that are for lines not constrained to pass through the origin have solid  
273 symbols and those for lines constrained to pass through the origin open symbols. The values  
274 of each generally reduce fairly consistently with  $p'$ . There is some scatter at higher stresses for  
275 isotropic compression because there were too few tests reaching these stresses, high pressure  
276 triaxial tests being rather more difficult to conduct than oedometers. As noted above, the effect  
277 of the constraint is significant for the oedometer tests on LBS, but less so for isotropic  
278 compression on the same soil. In each case a constraint to pass through the origin has the effect  
279 of increasing the gradient, which might be expected since the intercepts should not be negative  
280 because the current void ratio should always be lower than the initial value.

### 281 *Quantifying Convergence in Shearing*

282 For triaxial shearing similar gradients,  $m$ , were calculated at fixed values of shear strain, (0.1%,  
283 1%, 5%, 10%, 15%, 20% and 30%) grouping data for tests that have similar current  $p'$  values  
284 at those strains. Figure 8 shows the data for  $\epsilon_s^p=10\%$ . This is the plastic component of shear  
285 strain, the elastic component, which was very small, having been deducted based on elastic  
286 shear moduli from bender element data. For the calculation of the plastic volumetric strains,  
287  $\epsilon_v^p$ , that are used later, a Poisson's ratio of 0.3 was assumed in the absence of any measurements  
288 of the elastic bulk modulus. All of the unconstrained lines with intercepts as well as the lines

289 constrained to pass through the origin are shown, along with their equations, but examples are  
290 only given for a few stress levels in each figure for clarity, the calculation being repeated for  
291 other stress levels. In general the gradients of the lines,  $m$ , tend to reduce as stress level  
292 increases, although this is less clear for the LBS. The  $m$  values also decrease as the  $\epsilon_s^p$  increases,  
293 but space preclude showing more examples. Using this method, data points may be plotted for  
294 any stress path, and the data for drained and undrained tests are not highlighted on the plot,  
295 since they were indistinguishable. The use of lubricated end platens for some of the LBS tests  
296 does not have any noticeable effect within the data scatter, as highlighted in Fig.8a.

297 The data in Fig.8 are quite scattered, especially for the unconstrained gradients, even if 20-30  
298 triaxial tests were carried out for each soil. This gives some inconsistent trends in the change  
299 of  $m$  with  $p'$ . The  $m$  values are, however, lower than those for isotropic compression, as they  
300 should be since shearing can only give additional convergence beyond that achieved in the  
301 isotropic compression prior to shearing. The amount of test data needed to reduce the scatter  
302 significantly would therefore be prohibitive, so some form of data conditioning is needed.  
303 While it may be unfair to constrain the lines to pass through the origin, as discussed above,  
304 some form of constraint is required to avoid so much scatter in the shearing data.

### 305 *Applying Constraints to the Convergence Lines for Shearing*

306 It might be expected that the regression lines on Fig.8 that are not constrained to pass through  
307 the origin should move consistently as the shear strains increase. On Fig.9 the intercepts of  
308 these lines for all strain levels are given for the LMS, to give one example, showing data for  
309 all the stress levels considered, not just those that are on Fig.8b. At first sight the intercepts  
310 look quite scattered. This arises from small inaccuracies of void ratio measurement, even if this  
311 was carefully controlled and so was small. If the accuracy of void ratio cannot be improved,  
312 which would be difficult, then the only way to reduce this scatter of the intercepts is to carry

313 out even more tests, which becomes prohibitive. Nevertheless, there are important features in  
314 the data that can be seen. At each strain level a mean intercept is shown for all the stress levels.  
315 It might be expected that the intercepts should vary systematically rather than jumping  
316 randomly and it is noticeable that generally the mean values do vary quite consistently.  
317 However, the data have been further conditioned by drawing trends through the mean values,  
318 and it is these trend lines that were then used in the analysis. If these intercepts are constrained  
319 to vary systematically then the gradients will also. These trend lines on Fig.9 been assumed to  
320 be straight for convenience and because the data scatter does not allow a better choice. The  
321 trend lines have a few constraints, for example that they may not increase indefinitely or  
322 decrease below zero. Having chosen these lines, intercepts for the convergence lines are  
323 calculated for each value of shear strain from the line, not the mean value data point at that  
324 strain. New gradients  $m$  are then calculated forcing the regression lines on graphs like those  
325 shown in Fig.8 through the imposed intercept. These new lines that are forced through the  
326 chosen intercepts are not shown on Fig.8 to avoid clutter, but they are quite similar to the  
327 unconstrained lines.

328 The impact of the constraint to the intercept on the gradients  $m$  for the shearing data are  
329 illustrated for the LMS soil in Fig.10. The completely unconstrained values, identified with  
330 open symbol type data points are very scattered. A hard, and perhaps unrealistic constraint, of  
331 making all the chosen lines pass through the origin does of course give gradients that are much  
332 more consistent, as shown by the cross-type symbol data points. However, this constraint also  
333 changes the overall trend, increasing the  $m$  values significantly. Instead, the proposed “soft”  
334 constraint of imposing intercepts calculated from graphs like Fig.9 helps to reduce scatter while  
335 not changing the overall trends and values significantly, as shown by the grey filled data points.  
336 In each case, however, while  $m$  does reduce with increasing shear strain, the  $m$  values are far  
337 from reaching the value of zero which would indicate a unique critical state line in the  $e:\ln p'$

338 plane. Similar constraints to have consistently evolving intercepts on the regression lines used  
339 to calculate  $m$  could also be used for the oedometer and isotropic compression data, but it was  
340 not found necessary and the unconstrained values could be used.

#### 341 Convergence Surfaces

342 To compare the  $m$  values for different types of tests, the assumption made is that the degree of  
343 convergence will depend simply on the plastic volumetric and shear strains that are applied to  
344 the soil, and not on the apparatus applying them. A similar dependence on plastic strains is  
345 made in the damage functions that define the rates of destructuration for many models for  
346 natural soils (e.g. Kavvadas & Amorosi, 2000), which seems appropriate since the slow  
347 convergence is known to result from the difficulty in breaking down the initial fabric. The  
348 strains used are cumulative from the start of each test at  $p'=20\text{kPa}$  since it is the overall strain  
349 that the soil has experienced that should determine the breakdown of structure.

350 To construct a convergence surface a three-dimensional graph is drawn relating the  $m$  values  
351 to the plastic shear and volumetric strains,  $\epsilon_s^p$  and  $\epsilon_v^p$ , using all three methods of deriving  $m$ ,  
352 from isotropic compression, oedometric loading and triaxial shearing. This is shown for the  
353 LMS in Fig.11 using the  $m$  values that were constrained with the hard constraint so that the  
354 convergence lines for all types of loading all pass through the origin of the convergence graphs.  
355 This is shown in preference to the completely unconstrained data since the data for completely  
356 unconstrained  $m$  values are too scattered in shearing.

357 The resulting graph is difficult to understand and so an annotated version is shown in Fig11b.  
358 The graph is quantifying how quickly tests on samples of different initial void ratios approach  
359 convergence to unique void ratios, for example on a unique normal compression line (isotropic  
360 or one-dimensional) or unique critical state line, when  $m$  will be zero. Isotropic compression  
361 runs from the start of the surface at zero strains and  $m=1$  (no convergence yet) almost following

362 the zero shear strain axis. For isotropic compression tests estimates of the shear strains were  
363 calculated using the measured volumetric strains combined with the axial strains from the  
364 internal axial strain transducers, although those shear strains were of course very small.

365 For the oedometer tests the ratio of total volumetric to shear strains is fixed, and the path of the  
366 data points therefore lies diagonally across the graph at a ratio of strains of about  $2/3$  with  $m$   
367 decreasing as the tests proceed. The ratio is not quite  $2/3$  because here we plot plastic, not total  
368 strains. For the isotropic and oedometric compression each point represents all of the tests  
369 conducted on that soil and so a strain must be assigned to each the  $m$  values calculated, for  
370 example, from Fig.6b. The value chosen is the mean strain reached by all the tests at that stress  
371 level, since the variation between tests was not large.

372 The triaxial shearing data define a series of points at the chosen shear strain values, running  
373 across the graph with  $m$  decreasing as shear strain increases, while the volumetric strain also  
374 increases but by much less. The starting point for triaxial shearing is after isotropic compression  
375 has been applied, so the paths will start on the isotropic compression path, tests at lower stresses  
376 starting closer to the start of the graph at  $m=1$  and zero strains, while high pressure triaxial tests  
377 will have already had some significant reduction in  $m$  during isotropic loading.

378 A surface has been fitted through all of the data points and, given the data scatter, this has  
379 simply been assumed to be an inclined flat surface. To help visualisation in a two-dimensional  
380 image, firstly the coordinates of the corners of the surface are highlighted, and then the  
381 locations of the data points are clarified with a vertical line extending from each point to the  
382 surface, points lying below the surface having a solid line and those above a dashed one. In  
383 fitting the surface, least squares regression was used but weighting was applied to each data  
384 point for the number of tests used to derive it, so greater weight is given to the oedometer data  
385 points. The plane chosen has been constrained to pass through  $m=1$  at zero strains, as it must



386 do. There is no reason why the surface must be flat, and it would be expected, for example, that  
387 if it does approach  $m=0$  then it would become asymptotic to that boundary since it cannot cross  
388 it. But to define the precise curved shape would again require a very large number of tests and  
389 for the present purpose there are data both above and below the chosen plane, so it seems to be  
390 a reasonable choice.

391 Some of the LMS data plot with small negative  $\varepsilon_v^p$  values because the small plastic volumetric  
392 strains during isotropic compression were less than the dilation during shear. This illustrates  
393 one defect of the current formulation, which is that plastic straining should destructure whether  
394 it is positive or negative and some means of combining them better needs to be devised, which  
395 be, for example, some form of work done, but this is beyond the current scope and will not  
396 frequently be a problem for transitional soils that are generally compressive in shearing.  
397 However, a Cam Clay style work equation would be unlikely to work because the surface  
398 clearly shows that convergence from the breakdown of the initial fabric is brought about much  
399 more rapidly by volumetric than shear strains and in this respect is similar to some  
400 destructuration models for natural clays (e.g. Kavvadas & Amorosi, 2000).

401 Each type of test has its own defects and inaccuracies, for example wall friction in oedometer  
402 tests or in a triaxial the effects of end restraint or strain localisation. It was shown above that  
403 within the large differences of void ratio caused by lack of convergence, the effects of end  
404 restraint are not significant, but Fig.11 provides further confirmation that it is not test defects  
405 that inhibit reaching unique states since the  $m$  values at given strains are broadly similar for  
406 different types of test. The key feature of the plot is that the degree of “incompleteness” of the  
407 tests is explicit and it is clear, for example, that continued shearing in a triaxial test will not  
408 bring about convergence.

409 As was highlighted above, using constrained values of  $m$  with zero intercepts imposed, may  
410 not be a desirable assumption, even if the lines derived fit the data reasonably well in Figs.6  
411 and 8. Figure 12 therefore shows surfaces for all three soils that are plotted using the  $m$  values  
412 that are partially constrained or have the “soft” constraint for shearing. Here the completely  
413 unconstrained values are used for isotropic and oedometric compression, but for triaxial  
414 shearing the intercepts are constrained to change consistently, as in Fig.9. Relaxing the  
415 constraint in this way does make  $m$  more sensitive to shear strain for the LMS, but it is still the  
416 volumetric strain that dominates convergence. It can also be seen that at high shear strains the  
417 data points are tending to plot above the flat planes, indicating that they should perhaps curve  
418 to shallower gradients with respect to  $\epsilon_s^p$ . The key features of the graphs remain, though, that  
419 simple tests of the type carried out here, even at high pressures, will never bring about  
420 convergence, and will never give unique normal compression or critical state lines for these  
421 types of soil. If convergence were to be found, it would require enormous stress and/or strain  
422 levels, well beyond most engineering relevance and possibly so close to the zero void boundary  
423 as to make it difficult to define any useful normal compression or critical state line.

#### 424 Conclusion

425 Transitional behaviour is a controversial subject that can provoke entrenched positions, as have  
426 often been experienced by the authors. Not least, the name of this mode of behaviour is  
427 unhelpful as it risks confusion with other uses of “transitional” in soil mechanics, such as  
428 transitional fines content. The terminology is difficult to change and it may be that the two uses  
429 are related through the grading. The use of “transitional” here was originally supposed to  
430 indicate a transition between clay and sand modes of behaviour, although this has probably  
431 become obsolete as a justification as more examples are found. This paper has tried to present  
432 a means of quantifying rates of convergence towards unique volumetric states in compression  
433 or shearing, which should help focus the discussion. Using this method it is clear that for the

434 three soils presented there is no possibility that simple laboratory element tests such as triaxial  
435 or oedometer tests can get anywhere near full convergence of the volumetric states such as to  
436 give useful unique normal compression or critical state lines. It is also clear that this is not the  
437 result of defective testing techniques but must be related to the persistence of fabric effects, as  
438 highlighted by Todisco et al. (2018). If we wished to bring about that convergence we would  
439 need other apparatus able to impose very much larger strains and/or stress levels which may  
440 then have little relevance to engineering practice. Finally, while the soils tested here may be  
441 somewhat unlikely artificial soil gradings, it should be recalled that transitional behaviour has  
442 been observed in many natural soils and so this unifying method will be a useful new tool to  
443 interpret data from such soils. Of course the technique could also be used for soils that are not  
444 transitional, and would be useful in assessing how quickly unique normal compression lines or  
445 critical state lines are reached and in understanding whether data are consistent between  
446 different forms of loading.

#### 447 **ACKNOWLEDGEMENTS**

448 The authors are grateful to Dr. Barbara Shipton for the use of her data for the SPF soil.

449

450 **REFERENCES**

- 451 Altuhafi, F. N. & Coop, M. R. (2011). Changes to particle characteristics associated with the  
452 compression of sands. *Géotechnique*, 61 (6), 459-471.
- 453 Altuhafi, F., Baudet, B. A., & Sammonds, P. (2010). The mechanics of subglacial sediment:  
454 an example of new “transitional behaviour”. *Can. Geotech. J.*, 47 (7), 775-790.
- 455 Atkinson, J. H. & Evans, J. S. (1985). Discussion on: The measurement of soil stiffness in the  
456 triaxial apparatus, by Jardine, R. J., Symes, N. J. & Burland, J. B. *Géotechnique*, 35 (3), 378-  
457 382.
- 458 Coop, M.R. (2015) Limitations of a Critical State Framework Applied to the Behaviour of  
459 Natural and “Transitional” Soils. 6th Intl Symp. on Deformation Characteristics of  
460 Geomaterials, Buenos Aires, 115 – 155.
- 461 Coop, M.R. & Lee, I.K. (1993). The behaviour of granular soils at elevated stresses. Predictive  
462 Soil Mechanics, Proc. C.P.Wroth Mem Symp., Thomas Telford, London: , 186-198.
- 463 Cotecchia, F. & Chandler, R. J. (2000). A general framework for the mechanical behaviour of  
464 clays. *Géotechnique*, 50 (4), 431-447.
- 465 Coop, M.R., Sorensen, K.K., Bodas Freitas, T. & Georgoutsos, G., (2004). Particle breakage  
466 during shearing of a carbonate sand, *Géotechnique*, 54 (3), 157-163.
- 467 Fearon, R. E. & Coop, M. R. (2000). Reconstitution: what makes an appropriate reference  
468 material? *Géotechnique*, 50 (4), 471-477.
- 469 Ferreira, P. M. & Bica, A. V. D. (2006). Problems in identifying the effects of structure and  
470 critical state in a soil with a transitional behaviour. *Géotechnique*, 56 (7), 445-454.

471 Hosseini-Kamal, R., Brosse, A., Coop, M.R. & Jardine, R.J. (2014) The post-yield behaviour  
472 of four Eocene-to-Jurassic UK stiff clays. *Géotechnique*, 64(8), 620–634.

473 Kavvasdas, M. & Amorosi, A. (2000). A constitutive model for structured soils. *Géotechnique*,  
474 50 (3), 263-273.

475 Madhusudhan, B. N. & Baudet, B. A. (2014). Influence of reconstitution method on complete  
476 decomposed granite soil. *Géotechnique*, 64 (7), 540-550.

477 Martins, F. B., Bressani, L. A., Coop, M. R. & Bica, A. V. D. (2001). Some aspects of the  
478 compressibility behaviour of a clayey sand. *Can. Geotech. J.*, 38 (6), 1177-1186.

479 Nocilla, A., Coop, M. R. & Colleselli, F. (2006). The mechanics of an Italian silt; an example  
480 of “transitional” behaviour. *Géotechnique*, 56 (4), 261-271.

481 Ponzoni, E., Nocilla, A. & Coop, M. R. (2014). Identification and quantification of transitional  
482 modes of behaviour in sediments of Venice lagoon. *Géotechnique*, 64 (9), 694-708.

483 Ponzoni, E., Nocilla, A. & Coop, M. R. (2017) The behaviour of a gap graded sand with mixed  
484 mineralogy. *Soils & Foundations*, 57(6), 1030-1044.

485 Rocchi, I. & Coop, M. R. (2014). Experimental accuracy of the initial specific volume.  
486 *Geotech. Testing J., ASTM*, 37 (1), 169-175.

487 Santucci de Magistris, F., Silvestri, F. & Vinale, F. (1998). The influence of compaction on the  
488 mechanical behaviour of a silty sand. *Soils and Foundations*, 38 (4), 41-56.

489 Shipton, B. & Coop, M. R. (2012). On the compression behaviour of reconstituted soils. *Soils  
490 and Foundations*, 52 (4), 668-681.

491 Shipton, B. & Coop, M. R. (2015). Transitional behaviour in sands with plastic and non-plastic  
492 fines, *Soils and Foundations*, 55 (1), 1-16.

493 Takahashi, A. & Jardine, R. J. (2007). Assessment of standard research sand for laboratory  
494 testing, *Quarterly Journal of Engineering Geology and Hydrology*, 40 (1), 93-103.

495 Todisco, M. C., Coop, M. R. & Pereira, J-M (2018) Fabric characterisation in transitional soils.  
496 *Granular Matter*, 20: 20. <https://doi.org/10.1007/s10035-018-0786-1>

497 Ventouras, K. & Coop, M.R. (2009) On the behaviour of Thanet sand: an example of an  
498 uncemented natural sand. *Géotechnique*, 59(9), 727-738.

499 Vilhar, G., Jovicic, V. & Coop, M.R. (2013) The role of particle breakage in the mechanics of  
500 a non-plastic silty sand. *Soils & Foundations*, 53(1), 91-104.

501 Xiao, Y., Coop, M.R., Liu, H., Liu, H., & Jiang, J. (2016) Transitional behaviors in well-graded  
502 coarse granular soils. *J. Geotech and Geoenv. Engng.*, 142(12), 10.1061/(ASCE)GT.1943-  
503 5606.0001551.

#### 504 **NOMENCLATURE**

505	e	void ratio
506	$e_i$	initial void ratio
507	$k_0$	coefficient of earth pressure at rest
508	LBS	Leighton Buzzard sand
509	LMS	crushed limestone
510	M	stress ratio at critical state
511	m	convergence parameter
512	$p'$	mean normal effective pressure

- 513  $q$  deviatoric stress
- 514 SPF sand plastic fine (75% sand – 25% kaolin)
- 515  $\varepsilon_s$  shear strain ( $\varepsilon_s^p$  plastic component)
- 516  $\varepsilon_v$  volumetric strain ( $\varepsilon_v^p$  plastic component)
- 517  $\Gamma$  intercept of critical state in  $e:\ln p'$  plane at  $p'=1\text{kPa}$
- 518  $\lambda$  gradient of critical state or normal compression lines in  $e:\ln p'$  plane
- 519  $\phi'$  angle of shearing resistance
- 520  $\sigma'_v$  vertical effective stress

521

522 Table 1 Details of oedometer tests on LBS and LMS samples.

Type of soil	Initial void ratio, $e_i$	Final void ratio, $e_{\text{final}}$	Accuracy of the initial void ratio
LBS	0.597	0.322	$\pm 0.015$
	0.389	0.292	$\pm 0.019$
	0.534	0.303	$\pm 0.003$
	0.453	0.298	$\pm 0.012$
	0.411	0.291	$\pm 0.003$
	0.378	0.297	$\pm 0.001$
LMS	0.812	0.328	$\pm 0.017$
	0.611	0.253	$\pm 0.023$
	0.512	0.273	$\pm 0.002$
	0.537	0.317	$\pm 0.021$
	0.645	0.249	$\pm 0.005$
	0.511	0.202	$\pm 0.002$
	0.410	0.230	$\pm 0.007$
	0.431	0.248	$\pm 0.009$
	0.359	0.225	$\pm 0.005$

523

524 Table 2 Details of triaxial tests on LBS samples

Test no.	Initial void ratio, $e_i$	Void ratio end of shearing	$p'$ compression [kPa]	$p'$ end of shearing [kPa]	Accuracy of $e$
LBD1	0.582	0.484	100	180	$\pm 0.014$

LBD2*	0.583	0.472	500	930	±0.014
LBU3	0.555	0.500	500	460	±0.006
LBD4	0.551	0.466	500	940	±0.004
LBD5	0.524	0.445	500	950	±0.01
LBD6	0.544	0.461	1000	1830	±0.03
LBD7 <sup>+</sup>	0.472	0.443	100	190	±0.04
LBD8 <sup>+</sup>	0.435	0.422	100	200	±0.003
LBD9	0.420	0.411	100	190	±0.01
LBD10	0.435	0.369	300	550	±0.02
LBD11	0.497	0.420	500	990	±0.013
LBD12* <sup>+</sup>	0.457	0.386	500	1100	±0.007
LBD13	0.437	0.388	500	840	±0.007
LBU14	0.412	0.358	500	380	±0.01
LBD15	0.436	0.281	5300	9680	±0.003

525 \* sheared to less than 10% shear strain, <sup>+</sup> lubricated ends.

526

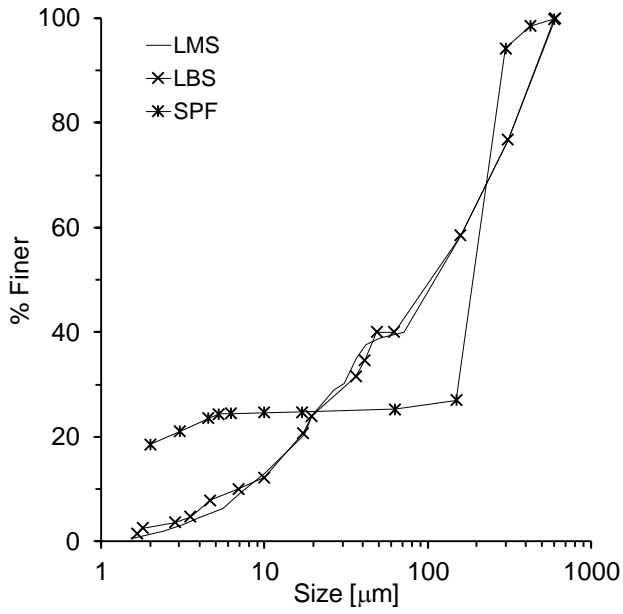
527 Table 3 Details of triaxial tests on LMS samples

Test no.	Initial void ratio, $e_i$	Void ratio end of shearing	$p'$ compression [kPa]	$p'$ end of shearing [kPa]	Accuracy of $e$
LMD1	0.605	0.555	50	80	±0.003
LMU2	0.607	0.520	720	475	±0.008
LMU3	0.548	0.511	95	40	±0.012
LMD4	0.549	0.453	300	650	±0.004
LMD5	0.506	0.432	300	610	±0.008
LMD6	0.538	0.410	570	1250	±0.022
LMD7	0.531	0.382	1020	2240	±0.010
LMD8	0.513	0.341	3080	6250	±0.007
LMD9	0.445	0.453	50	130	±0.01
LMD10	0.415	0.416	50	130	±0.007
LMU11	0.409	0.405	50	750	±0.007
LMD12	0.464	0.422	100	170	±0.026
LMD13	0.395	0.373	200	930	±0.002
LMD14	0.388	0.368	200	490	±0.002
LMD15*	0.492	0.389	500	520	±0.05
LMD16	0.471	0.356	470	1050	±0.012
LMD17	0.425	0.387	500	1140	±0.005
LMU18	0.390	0.356	500	1630	±0.007
LMD19	0.415	0.288	2400	5100	±0.01
LMD20	0.373	0.234	3880	7860	±0.009
LMD21	0.350	0.300	1000	2150	±0.008

528 \*constant  $p'$  shearing.

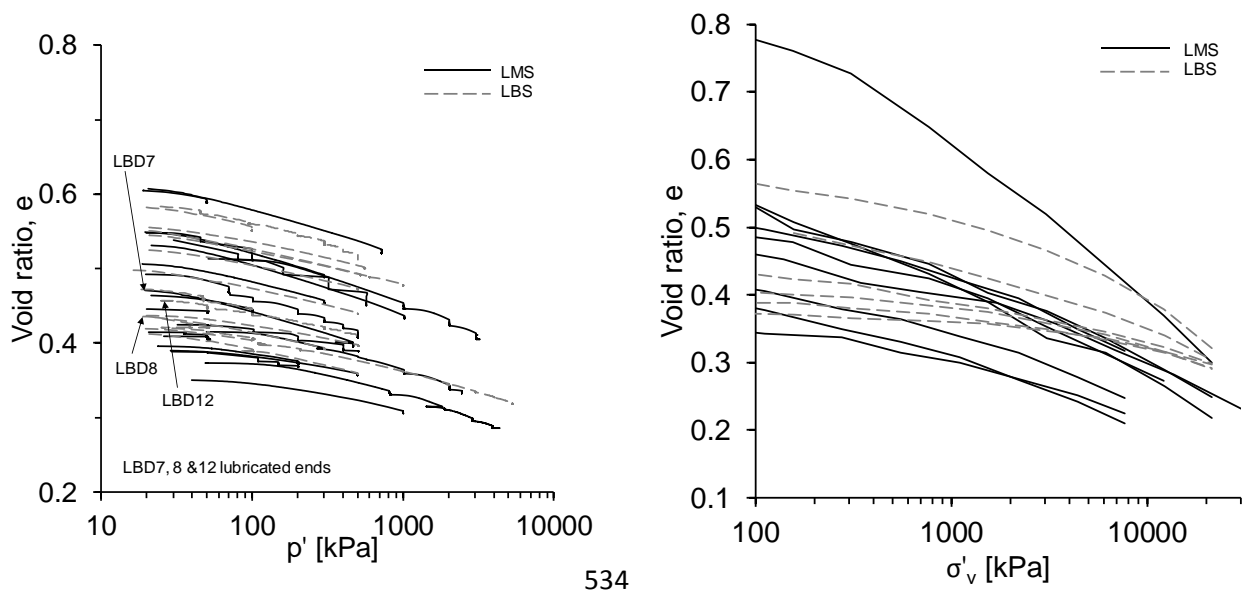
529





530

531 Fig.1 Gradings of the three soils.



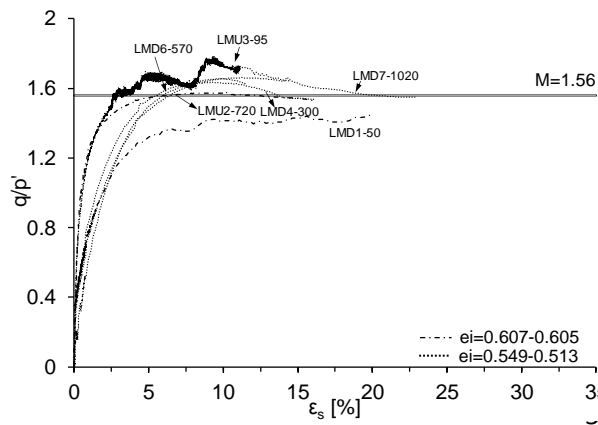
532

534

533 (a)

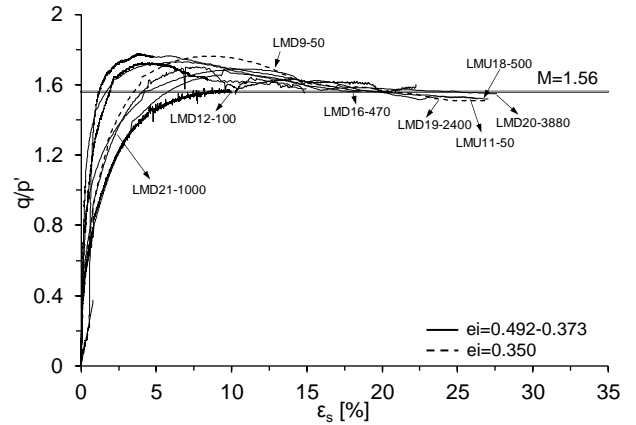
535 (b)

536 Fig.2 Compression data for LMS and LBS soils, (a) isotropic, (b) oedometric

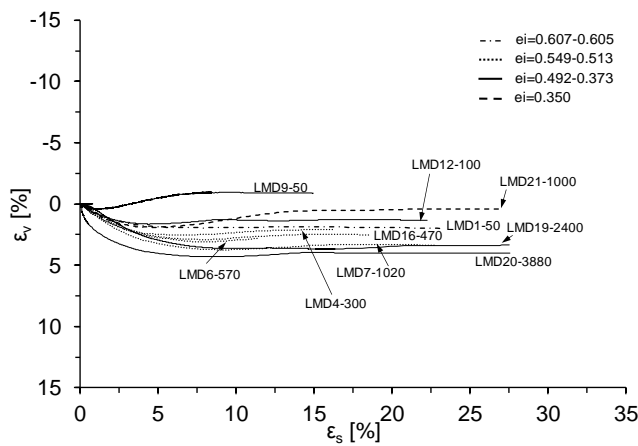


537

538 (a)



540 (b)

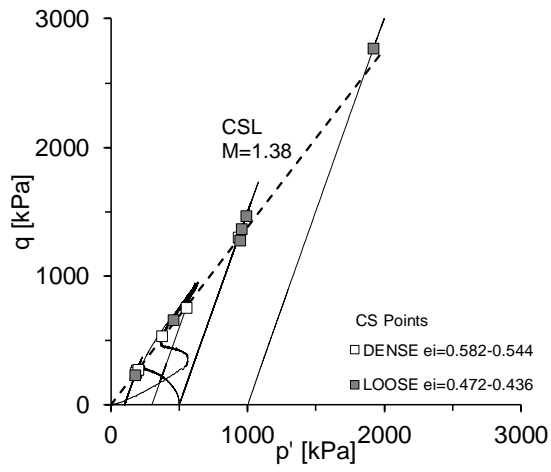


541

542 (c)

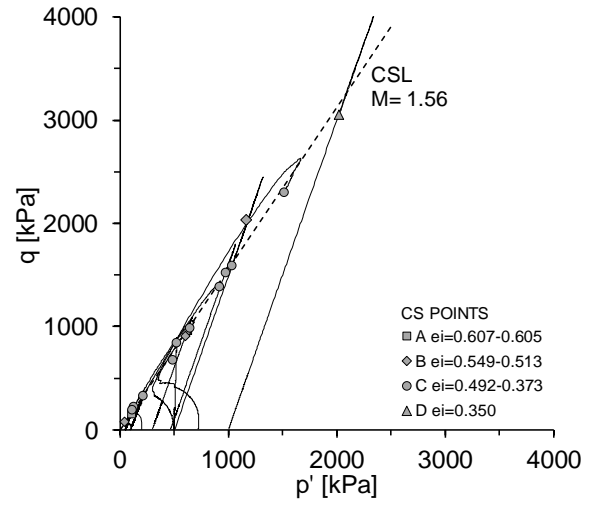
543 Fig.3 Example triaxial stress-strain data for the LMS soil, (a) stress ratio for looser samples,  
 544 (b) stress ratio for denser samples, (c) volumetric strains for drained tests on samples of all  
 545 densities.

546



547

548 (a)

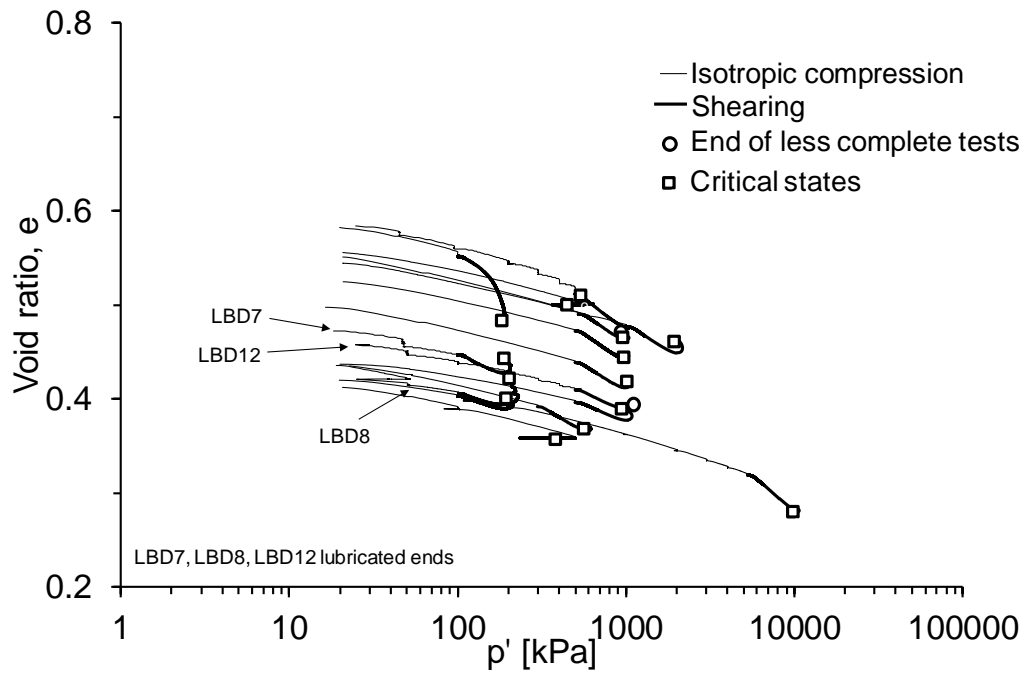


549

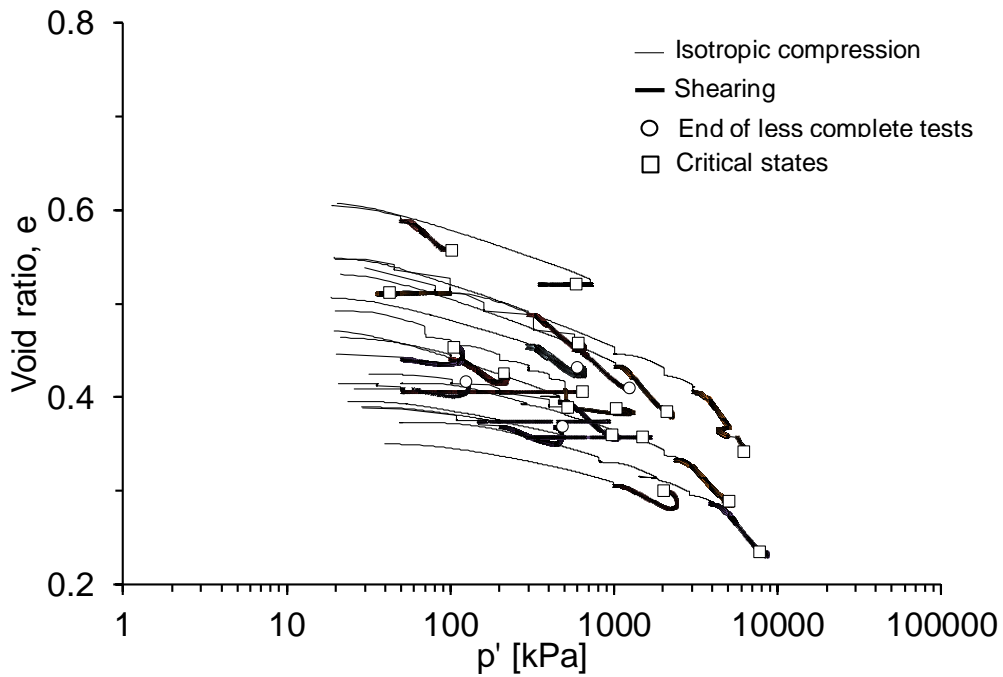
550 (b)

551 Fig.4 Stress paths (a) LBS (b) LMS

552

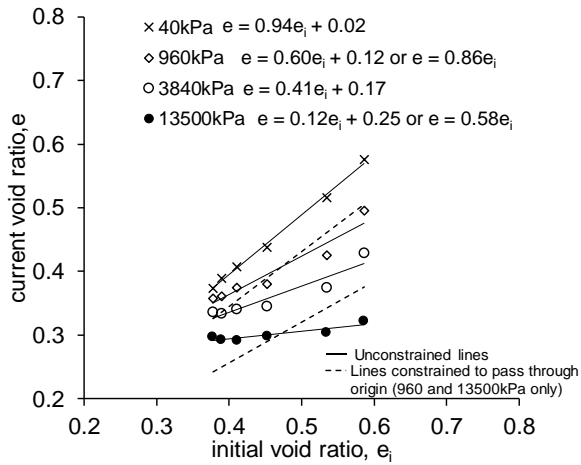


555 (a)



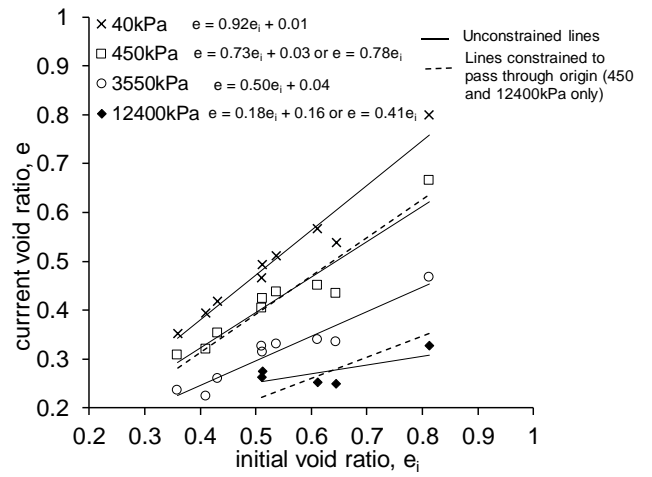
557 (b)

558 Fig.5 Paths followed in the volumetric plane (a) LBS (b) LMS



561

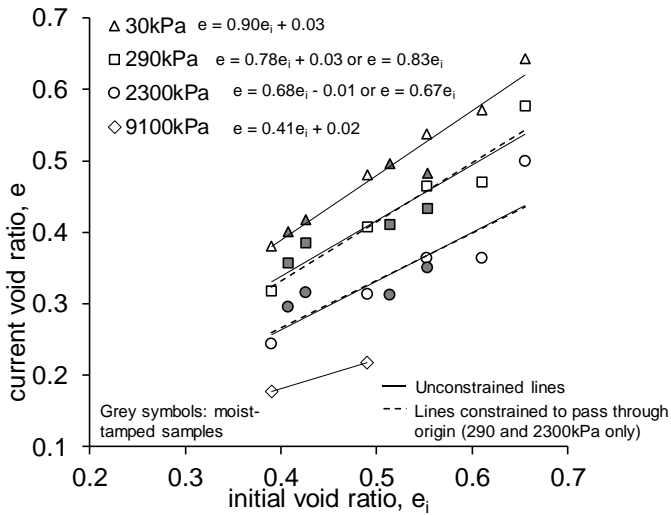
562 (a)



563

564 (b)

565

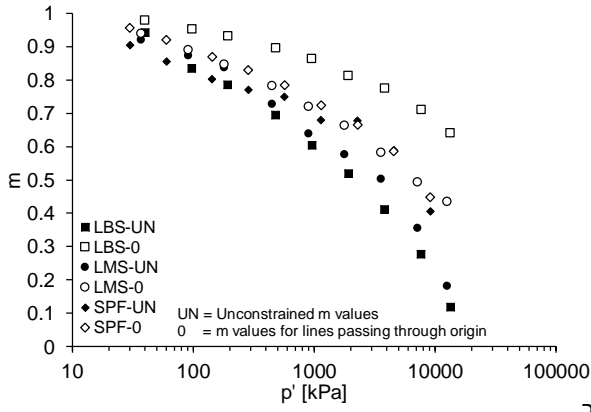


566

567 (c)

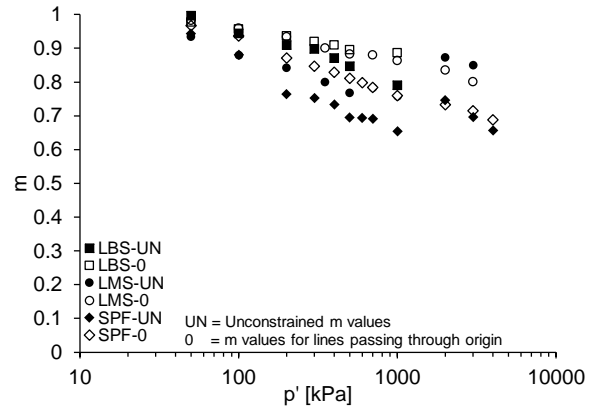
568 Fig.6 Convergence lines for oedometer tests on the three soils, (a) LBS, (b) LMS and (c) SPF

569



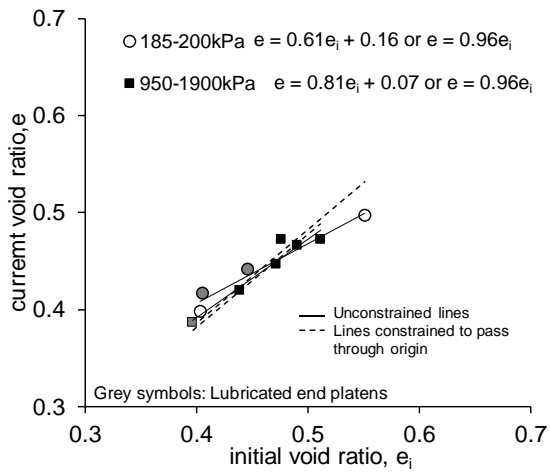
570

571 (a)



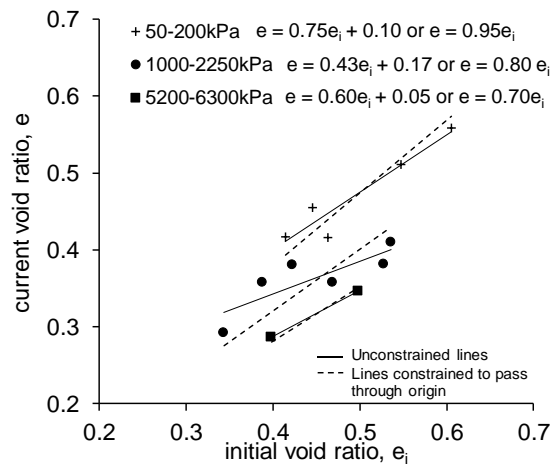
573 (b)

574 Fig.7 Summary of m values for (a) one-dimensional and (b) isotropic compression



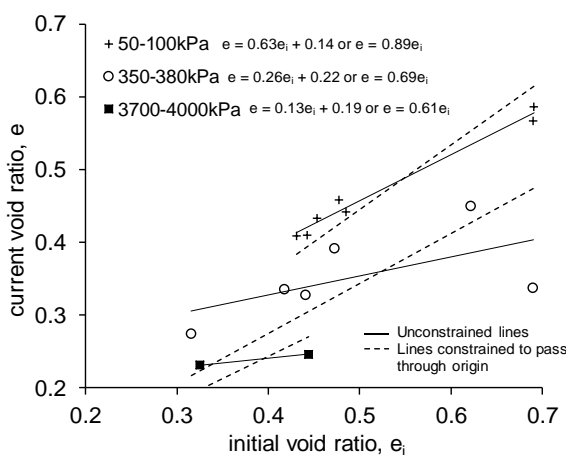
575

576 (a)



577

578 (b)

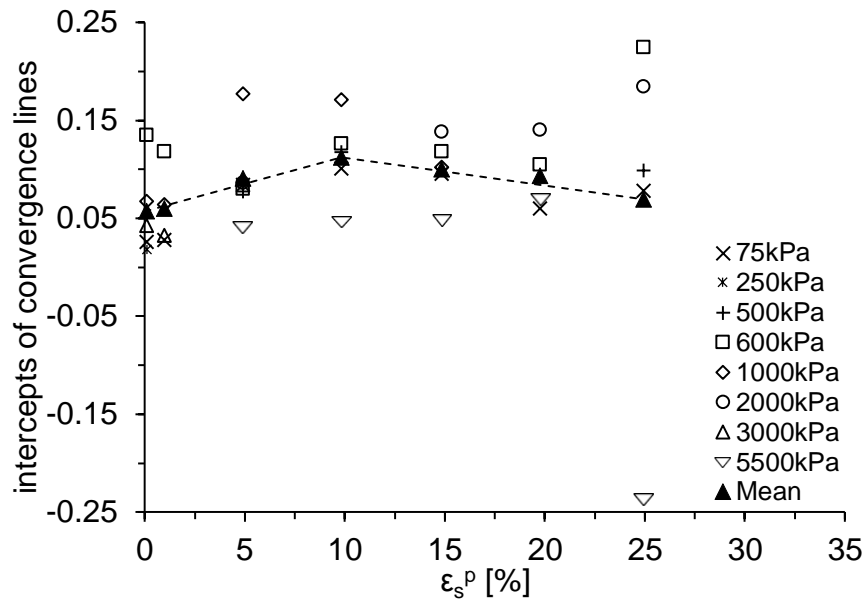


579

580 (c)

581 Fig.8 Convergence lines at  $\epsilon_s^p = 10\%$  during triaxial shearing of the three soils, (a) LBS, (b)

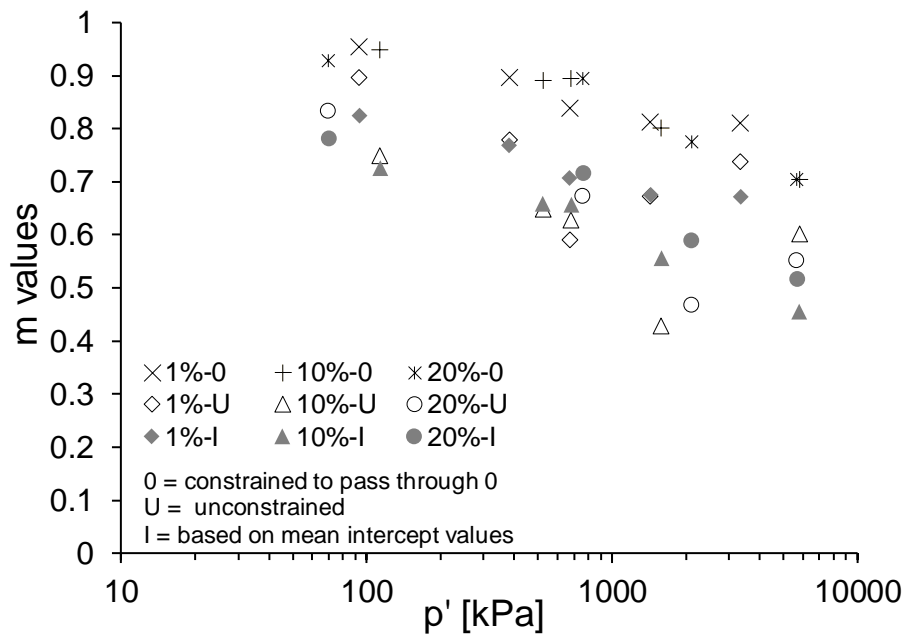
582 LMS and (c) SPF



583

584 Fig.9 Evolution of intercepts of shearing convergence lines with shear strain for LMS.

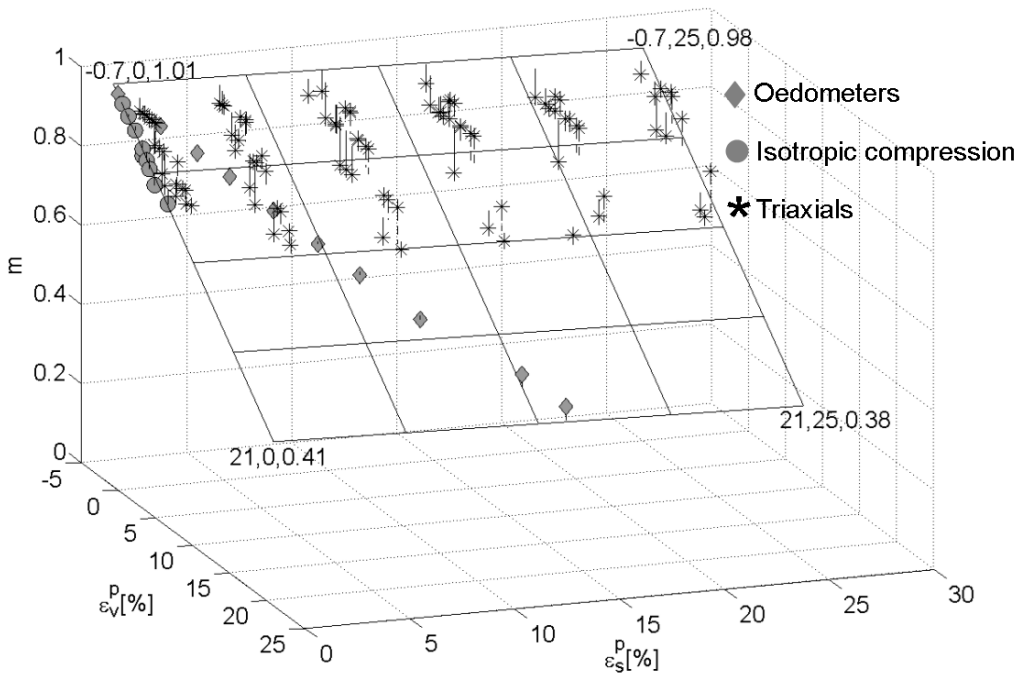
585



586

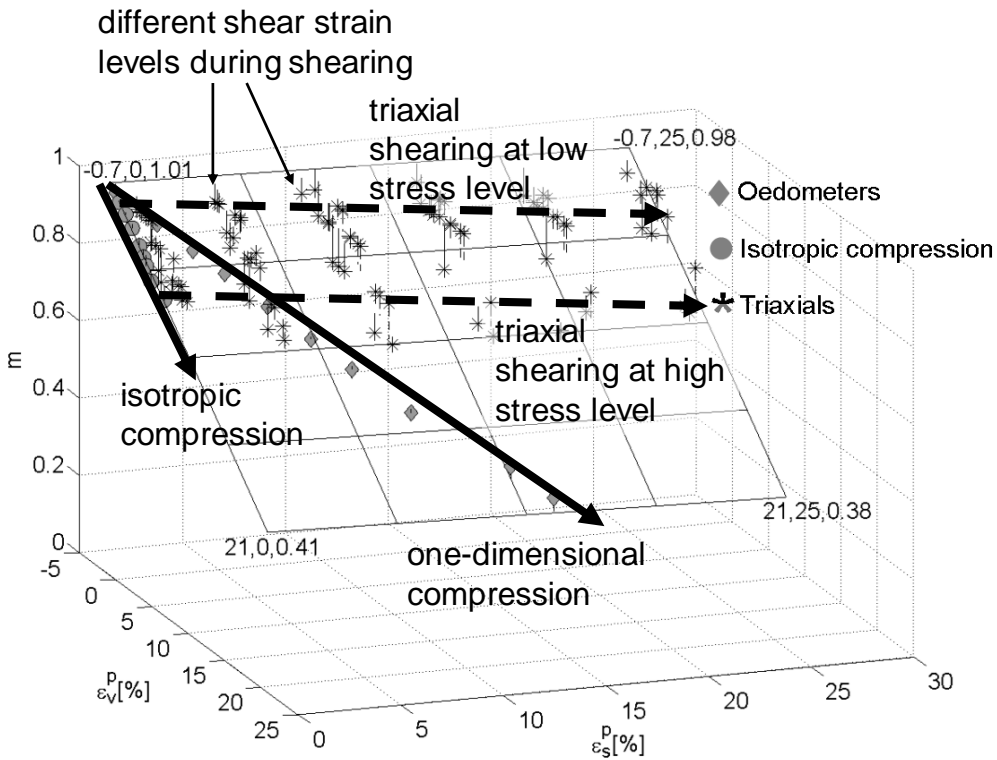
587 Fig.10 Evolution of shearing m values with stress level and shear strain for LMS.

588



589

590 (a)

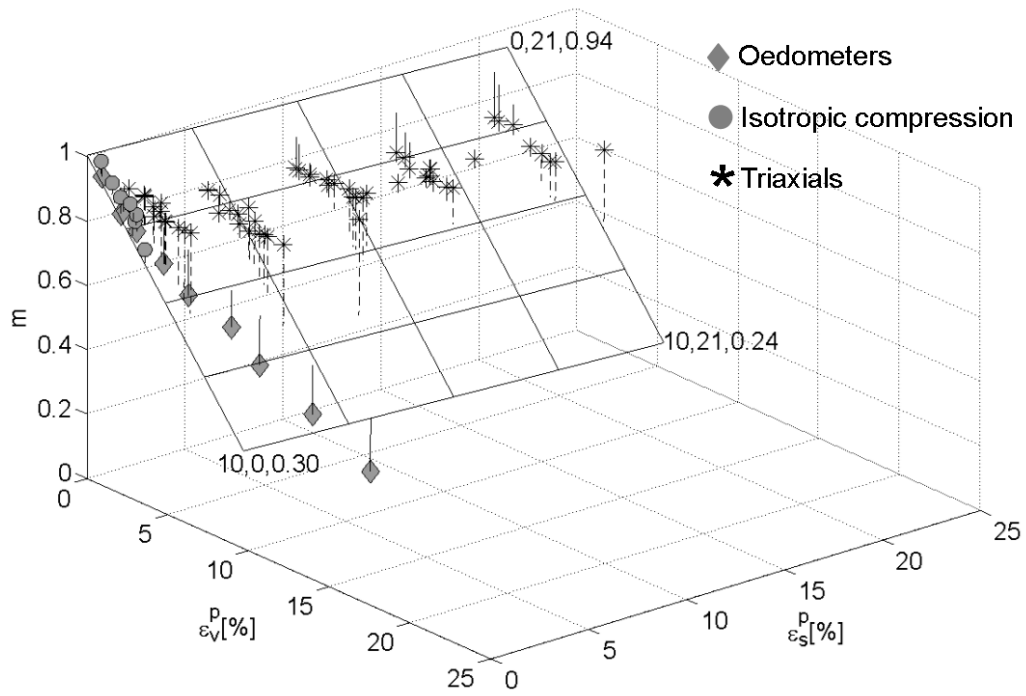


591

592 (b)

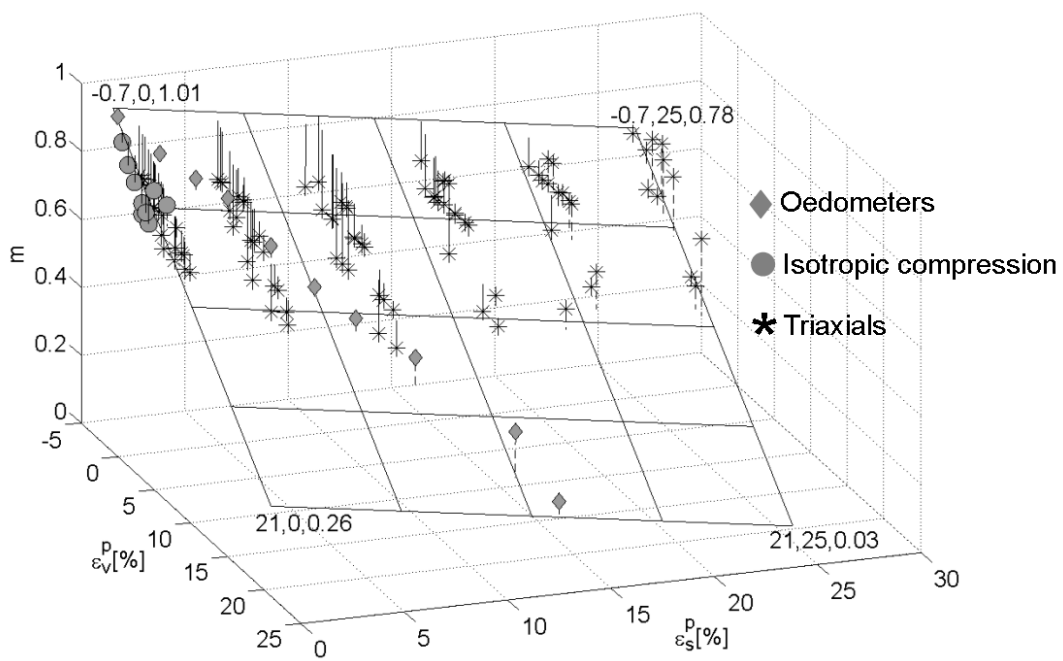
593 Fig. 11 (a) Convergence surface for constrained m values of LMS, (b) surface with  
 594 explanatory annotation.





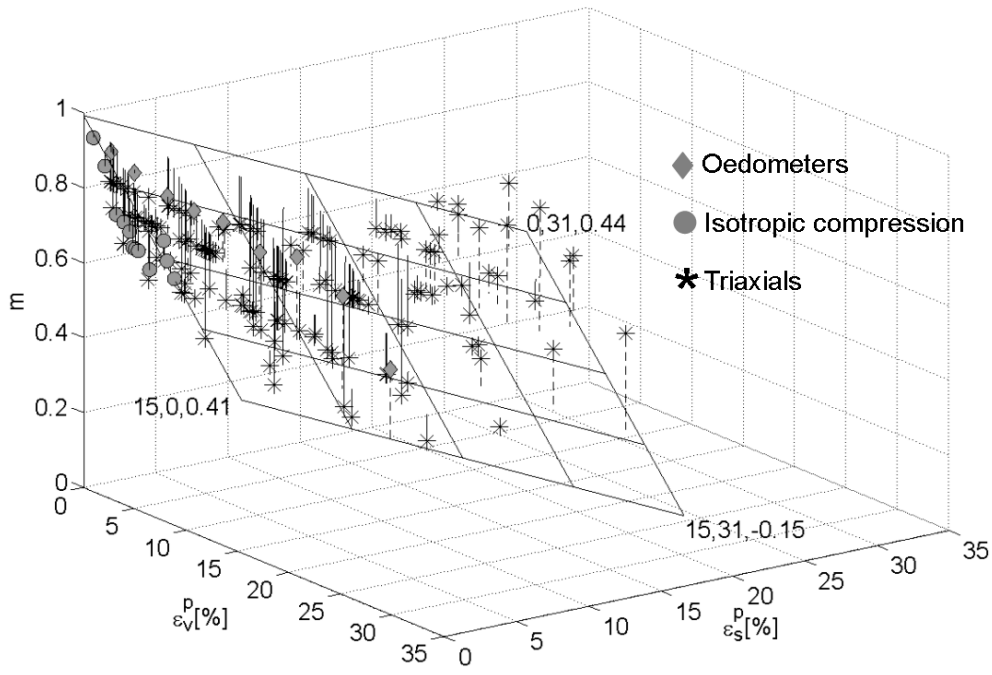
595

596 a)



597

598 b)



599

600 c)

601 Fig.12 Convergence surfaces with partial unconstraint of  $m$  values, a) LBS, b) LMS and c)

602 SPF.